Journal of Materials Science and Chemical Engineering, 2025, 13(11), 48-78
https://www.scirp.org/journal/msce
ISSN Online: 2327-6053
ISSN Print: 2327-6045

Evaluation of the Theoretical Design and Mathematical Modeling for Determination of Thermal and Viscous Irreversibilities in Axially Finned Two-Phase Closed Thermosyphon Heat Exchanger

Élcio Nogueira[1], Felix dos Santos Filho Diniz[2,3], Ryan Felix[1], Eliseu Luan de O. Tavares[3]

[1]Universidade do Estado do Rio de Janeiro (UERJ), Resende, Brazil
[2]Centro Universitário de Volta Redonda (UniFOA), Volta Redonda, Brazil
[3]Centro Universitário DomBosco Resende (AEDB), Resende, Brazil
Email: elcio.nogueira@uerj.br

How to cite this paper: Nogueira, É., Diniz, F. dos S.F., Felix, R. and Tavares, E.L. de O. (2025) Evaluation of the Theoretical Design and Mathematical Modeling for Determination of Thermal and Viscous Irreversibilities in Axially Finned Two-Phase Closed Thermosyphon Heat Exchanger. *Journal of Materials Science and Chemical Engineering*, **13**, 48-78.
https://doi.org/10.4236/msce.2025.1311005

Received: October 18, 2025
Accepted: November 22, 2025
Published: November 25, 2025

Abstract

Heat exchangers using thermosyphons have been used for decades in various applications in the aeronautical, military, nuclear, and electronics industries. One application that has gained recent interest, despite having been proposed around 1992, is thermal comfort in air conditioning systems. In this paper, we present a heat exchanger design that uses axially finned thermosyphons—AFTHE. The current design uses a radially finned heat pipe heat exchanger as a reference, whose theoretical and experimental analysis is already well established. Mathematical modeling applies to the thermal efficiency method to determine quantities of thermal interest, and the second law of thermodynamics, with an emphasis on the Bejan number, to determine thermal and viscous irreversibilities. Numerical and graphical results are determined and presented for the following physical quantities: velocities, Reynolds numbers, Nusselt numbers, convection heat transfer coefficients, number of thermal units, heat transfer rates, friction factors, pressure drops, and Bejan number. The results are used for theoretical analyses of the heat exchanger's evaporator and condenser, demonstrating the expected physical consistencies for all analyzed quantities. To consolidate the heat exchanger theoretical design and the applied theoretical model, a comparison is presented for the air outlet temperatures and effectiveness, using theoretical-experimental results obtained for the radial-fin heat exchanger, in the evaporator, and the condenser. The comparisons made demonstrate that the axially finned tube design presents better

thermal performance with a lower heat exchange area than the radially finned heat pipe design, for the same inlet conditions. The current design presents promising results and should be used in the experimental implementation of an air conditioning system for surgical rooms.

Keywords

Heat Exchangers, Axially Finned Heat Pipes, Thermal Efficiency Method, Thermal and Viscous Irreversibilities, Bejan Number

1. Introduction

Finned heat pipe heat exchangers (FHPHE) have been the subject of study and analysis, both theoretical and experimental, by several international research groups. These heat exchangers have a wide range of applications, notably in air conditioning systems for surgical rooms, which require strict specifications for temperature, air flow, relative humidity, and number of air changes per hour.

In this work, the thermal efficiency method is applied to determine the crucial thermal quantities for thermal performance. The main thermal quantity obtained through the application of the thermal efficiency method is the thermal effectiveness, which allows the determination of all other relevant thermal quantities for thermal performance analysis. The concept used in defining thermal efficiency is the concept associated with the definition of finned thermal performance, called "Fin Analogy". The concept of fin analogy was presented by Ahamad Fakheri [1]. Another relevant thermal quantity is thermal irreversibility, associated with viscous irreversibility, allows the determination of the overall performance of the heat exchanger.

The so-called "Bejan Number" [2] defines how efficient the heat exchanger is. In this sense, the weight of thermal irreversibility must be relatively greater than that of viscous irreversibility, so that the Bejan number is high.

Ragil Sukarno and colleagues [3] developed an experimental HVAC system for surgical rooms using finned crossflow heat pipe heat exchangers. They achieved a maximum efficiency of 62.7% for the nine-row, 36-finned-tube heat exchanger shown in **Figure 1** below, for an inlet temperature of 45˚C.

H. Jouhara and collaborators [4] conducted a theoretical experimental study to analyze the thermal performance of a multipass heat pipe heat exchanger using theoretical models such as Logarithmic Mean Temperature Difference (LMTD) and the Effectiveness Method (ε-NTU). They highlighted the importance of heat exchangers in waste energy recovery.

Grzegorz Górecki and collaborators [5] presented a theoretical-experimental study of a finned heat pipe heat exchanger for small air conditioning systems, showing that finned heat pipes are a viable alternative to conventional exchangers.

Anwar Barrak [6] discussed the rising energy consumption in tropical countries

and the importance of energy recovery to improve thermal performance. He highlighted that heat pipes are an excellent alternative for energy recovery and can improve fresh air quality.

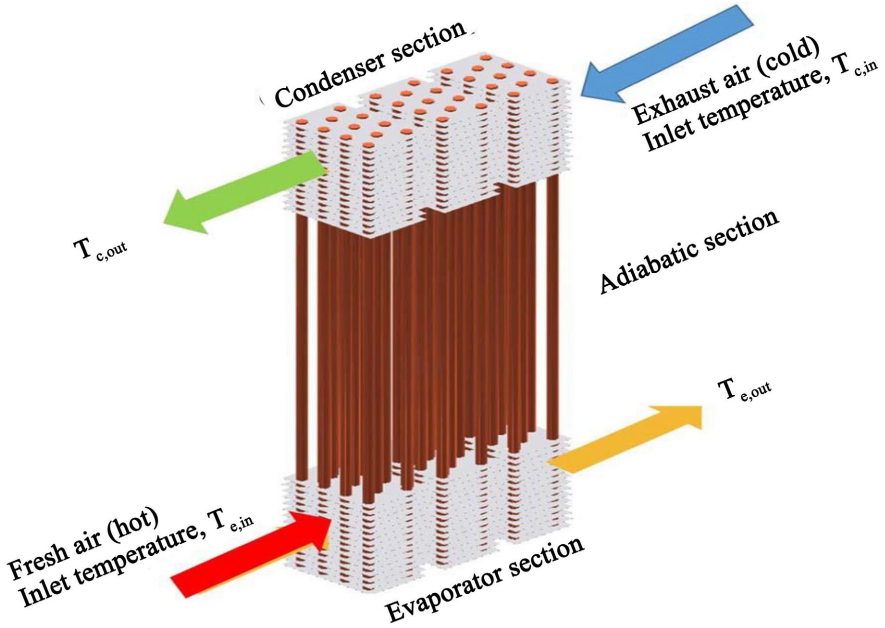

Figure 1. Ragil Sukarno *et al.* [3].

Nandy Putra and colleagues [7] investigated the performance of finned heat pipes for heat recovery from exhaust air in an ambient room, showing that system efficiency increases with inlet air temperature.

Imansyah Ibnu Hakim and colleagues [8] analyzed HVAC systems using U-shaped finned heat exchangers, concluding that the two-tube row configuration significantly affects the pre-cooling and reheating processes.

Xuan Yin *et al.* [9] use experimental data as a numerical simulation to calculate the operating states of a two-phase thermosyphon evaporator. The numerical model comprised a vertically arranged steel tube with an inner diameter of 17 mm and a length of 800 mm, and water as the working fluid. Seven heat exchange tubes in the evaporator are distributed in a uniform vapor environment. The numerical results reveal the heat transfer and flow characteristics in the tube at different filling rates, with the evaporator exhibiting different flow and heat transfer characteristics under filling rates ranging from 40% to 65%. At a tube height of 0.7 m, the distributions of time-averaged vapor velocity and void fraction are similar for filling rates ranging from 55% to 65%, indicating a similar flow regime. The applicability of the numerical model is validated by the experimental results.

H. Eshwar, U.C. Arunachala, and K. Varun [10] state that passive heat transport has gained immense popularity. They cite heat pipes (HP) and two-phase closed thermosyphons (TPCT). They evaluated the effectiveness of closed two-phase thermosyphons through experimental investigation. Three thermosyphons (with the same geometry) were analyzed. They imposed isothermal (40˚C - 90˚C) and

isoflux (50 - 900 W) heating conditions. They concluded that in isothermal mode, the HP transports heat with a minimal temperature gradient and that, ultimately, the HP is the preferred option in terms of performance. Due to its superior operation, the HP can be used in isothermal applications where cost is not a significant concern.

Élcio Nogueira [11] analyzed energy efficiency in air conditioning systems by applying the "Thermal Efficiency Method" to evaluate the thermal performance of finned heat pipe heat exchangers. The parameters analyzed included the number of fins per tube, number of tubes, inlet temperatures, and fluid flow rates. The theoretical results were compared with experimental data, showing excellent agreement.

Another study, Nogueira [12] reviewed concepts of thermal and viscous irreversibilities, using the second law of thermodynamics and the Bejan number to analyze the thermal and viscous performance of heat exchangers. The "Thermal Efficiency Method" was applied to obtain quantities such as thermal effectiveness and thermal and viscous irreversibilities.

Nogueira [13] also developed an innovative theory for analyzing heat exchangers, applying dimensionless analytical modeling to various types of exchangers, regardless of their specific characteristics. The methodology is based on the concepts of thermodynamics, with an emphasis on the second law of thermodynamics.

2. Basic concepts of Axially Finned Two-Phase Closed Thermosyphon Heat Exchanger—AFTHE

Some initial concepts of the axially finned tube heat exchanger with parallel flow in the evaporator and counterflow in the condenser are represented in **Figures 2(a)-(c)**.

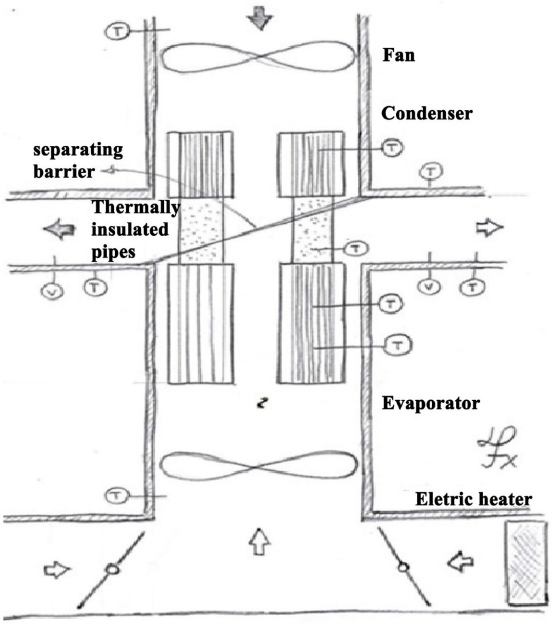

(a)

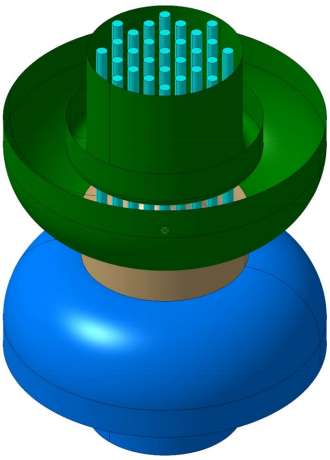

(b)

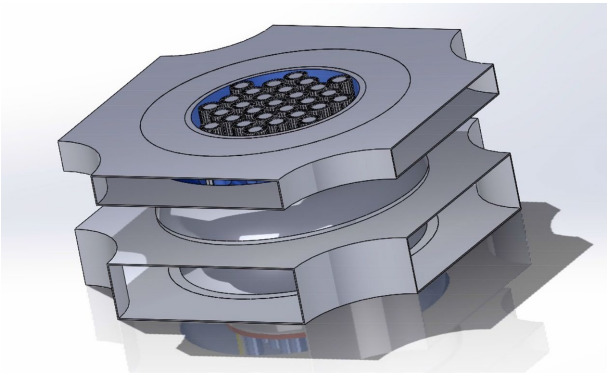

(c)

Figure 2. Basic initial concepts of AFTHE

Diniz Felix dos Santos Filho presents the initial design for the AFTHE (**Figure 2(a)**), highlighting the fin designs and an initial proposal for air outlets in the evaporator and condenser. Eliseu Luan de O. Tavares (**Figure 2(b)**), under the guidance of Élcio Nogueira, develops a new design for the heat exchanger, without fins, highlighting the vertical, diametrically symmetrical air outlets in the evaporator and condenser. Continuing the AFTHE concepts (**Figure 2(c)**), Ryan Felix expands the heat exchanger design with radial air outlets for the evaporator and condenser.

An analysis of the above designs for the AFTHE will be presented in the section below, considering theoretical aspects that will be discussed in the following sections.

3. Mathematical Model Description of the AFTHE

In this section we present the mathematical formulation for solving the performance of the heat exchanger under analysis, through the Thermal Efficiency Method, which uses the concept called "Fin Analogy" by Ahamad Fakheri [1].

The saturation temperature of the working fluid (H_2O) is defined using Equa-

tion (1).

$$T_{sat} = 27^{\circ}\text{C} \tag{1}$$

The air inlet temperature at the evaporator varies between 30˚C and 45˚C, according to Equation (2).

$$30^{\circ}\text{C} \le T_{airin} \le 45^{\circ}\text{C} \tag{2}$$

The air inlet temperature at the condenser varies between 18˚C and 26˚C, according to Equation (3).

$$18^{\circ}\text{C} \le T_{airin} \le 26^{\circ}\text{C} \tag{3}$$

The air mass flow rate varies between 0.02 kg/s and 0.15 kg/sec, according to Equation (4).

$$0.02\ \text{kg/s} \le \dot{m}_{air} \le 0.15\ \text{kg/s} \tag{4}$$

Table 1 shows the properties of the working fluid as a function of the saturation temperature equal to 27˚C.

Table 1. Working fluid properties (H_2O)

T_{sat} ˚C	P_{sat} Pa	ρ_l kg/m³	ρ_v kg/m³	h_l J/kg	h_v J/kg	h_{lv} J/kg
27.0	91.535 10^3	819.38	0.075	111.55	2563.19	2451.64

Geometric and physical quantities for the heat exchanger are explained through Equations (5) and (24).

$$D_{int} = \left(2.0 * 25.40\right)\text{mm} \tag{5}$$

The internal diameter of the heat pipe is represented by Equation (5).

$$D_{ext} = \left(2.0 * 25.40 + 0.893\right)\text{mm} \tag{6}$$

The external diameter of the heat pipe is represented by Equation (6).

$$P_{HP} = \pi * D_{ext} \tag{7}$$

The perimeter of the heat pipe is represented by Equation (7).

$$Esp_{Fin} = \left(P_{HP} - N_{Fin} * T_{Fin}\right) / \left(N_{Fin} + 1.0\right) \tag{8}$$

The space between fins is represented by Equation (8). The number of fins is represented by N_{Fin} and T_{Fin} represents the fin thickness.

$$N_{Fin} = 25 \tag{9}$$

$$T_{Fin} = 4.0\ \text{mm} \tag{10}$$

The basic reference number of heat pipes is represented by Equation (11). The reference number has an exact quadratic root and, in this work, is equal to 9 for 29 heat pipes and 16 for 47 heat pipes.

$$N_{HPb} = 9 \text{ by default;} \quad 1 \le N_{Hpb} \le 16 \tag{11}$$

The number of tubes in the main diagonal of the heat exchanger is represented

by Equation (12) (see **Figure 2**).

$$N_{HPR} = N_R + \left(N_R + 1.0\right) \tag{12}$$

where,

$$N_R = \sqrt{N_{HPb}} \tag{13}$$

The number of heat pipes is represented by Equation (14).

$$N_{HP} = N_{HPR} * \left(N_R + 1.0\right) + \left(N_R - 2.0\right) \tag{14}$$

The total number of fins in the heat exchanger is represented by Equation (15).

$$N_{TotFin} = N_{HP} * N_{Fin} \tag{15}$$

The fin height is represented by Equation (16).

$$H_{Fin} = 18.0 \text{ mm} \tag{16}$$

The diameter of the heat exchanger shell is represented by Equation (17).

$$D_{Shell} = N_{HPR} * \left(D_{ext} + 2.0 * H_{Fin}\right) \tag{17}$$

The lengths of the regions in the heat pipe, evaporator, adiabatic region and condenser are represented by Equation (18).

$$L_{Ev} = 220.0 \text{ mm};\ L_{Ad} = 120.0 \text{ mm};\ L_{Cd} = 120.0 \text{ mm} \tag{18}$$

$$L_{liqEv} = F_{Ratio} * L_{Ev} \tag{19}$$

The filling rate of the working fluid in the evaporator depends on the fraction ratio, defined by F_{Ratio} in Equation (19) above.

It is assumed that the heat pipes and fins are made of copper, with thermal conductivity shown below (Equation (20)).

$$k_W = 380.0 \frac{\text{W}}{\text{m} \cdot \text{K}}; k_{Fin} = 380.0 \frac{\text{W}}{\text{m} \cdot \text{K}} \tag{20}$$

Equation (21), represented by σ_{Water} and reported by Górecki, G. *et al.* [5], is the surface tension for water:

$$\sigma_{Water} = 0.07275 * \left(1.0 - 0.002 * \left(K - 291\right)\right) \tag{21}$$

where K is saturation temperature in Kelvin.

The air passage area at the heat exchanger inlet is represented by Equation (22).

$$AEnt_{HE} = \pi * \frac{D_{Shell}^2}{4.0} \text{ m}^2 \tag{22}$$

The height of the heat pipes is represented by Equation (23).

$$H_{HP} = L_{Ev} + L_{Ad} + L_{Cd} \tag{23}$$

The volume occupied by the heat pipes is represented by Equation (24).

$$Vol_{HE} = H_{HP} * AEnt_{HE} \tag{24}$$

The value 0.006 (Equation (25)), constant for the surface-fluid combination, was originally presented by Rhosenow [14], valid for the copper-water pair, and reported by H. Jouhara *et al.* [15].

$$C_{sf} = 0.006 \tag{25}$$

3.1. Evaporator

Table 2 shows the air properties as a function of the air inlet temperature at the evaporator.

Table 2. Air properties as a function of evaporator air inlet temperature.

T_{airin} °C	ρ_{air} Kg/m³	k_{air} W/(m·K)	Cp_{air} J/(kg·K)	Pr_{air}	μ_{air} Pa·s	ϑ_{air} m²/s	α_{air} m²/s
30.0	1.219	2.67×10^{-2}	1005.77	7.47×10^{-1}	1.98×10^{-5}	1.63×10^{-5}	2.18×10^{-5}
35.0	1.219	2.70×10^{-2}	1006.12	7.41×10^{-1}	1.99×10^{-5}	1.63×10^{-5}	2.20×10^{-5}
40.0	1.219	2.74×10^{-2}	1006.48	7.35×10^{-1}	2.00×10^{-5}	1.64×10^{-5}	2.23×10^{-5}
45.0	1.218	2.77×10^{-2}	1006.84	7.30×10^{-1}	2.01×10^{-5}	1.65×10^{-5}	2.26×10^{-5}

The air passage area inside the heat exchanger is represented by Equation (25).

$$Asec_{NHp} = AEnt_{HE} - \left(N_{HP} * \pi * \frac{D_{ext}^2}{4.0} - N_{TotFin} * H_{Fin} * T_{Fin} \right) \tag{25}$$

The hydraulic perimeter of the heat exchanger is represented by Equation (26).

$$P_{hHp} = N_{HP} * P_{HP} + N_{TotFin} * \left(2.0 * H_{Fin} + T_{Fin} \right) - N_{TotFin} * H_{Fin} \tag{26}$$

The hydraulic diameter of the heat exchanger is represented by Equation (27).

$$D_{hHP} = \frac{4.0 * Asec_{NHp}}{P_{hHp}} \tag{27}$$

The heat exchange area associated with the fins is represented by Equation (28).

$$A_{trFin} = N_{Fin} * N_{HP} * L_{EV} * \left(2.0 * H_{Fin} + T_{Fin} \right) \tag{28}$$

The heat exchange area associated with the heat pipe assembly is represented by Equation (29).

$$A_{trEv} = L_{EV} * N_{HP} * \left(P_{HP} - N_{Fin} * T_{Fin} \right) \tag{29}$$

The total heat exchange area in the evaporator is represented by Equation (30).

$$A_{totEv} = A_{trFin} + A_{trEv} \tag{30}$$

The Reynolds number associated with the air flow inside the evaporator is represented by Equation (31).

$$Re_{AirEv} = \frac{4.0 * \dot{m}_{air}}{\pi * D_{hHP} * \mu_{air}} \tag{31}$$

The air velocity inside the evaporator is represented by Equation (32).

$$V_{AirEv} = \frac{Re_{AirEv} * \mu_{air}}{D_{hHP}} \tag{32}$$

The Reynolds number associated with the air flow at the evaporator inlet is represented by Equation (33).

$$Re_{AirEnt} = \frac{4.0 * \dot{m}_{air}}{\pi * D_{Shell} * \mu_{air}} \tag{33}$$

The air velocity at the evaporator inlet is represented by Equation (34).

$$V_{AirEnt} = \frac{Re_{AirEnt} * \mu_{air}}{D_{Shell}} \tag{34}$$

The saturation temperature difference across the evaporator is represented by Equation (35).

$$\Delta T_{Evsat} = T_{airin} - T_{sat} \tag{35}$$

The estimated heat transfer coefficient for the boiling process, h_{boil}, Equation (36), was represented by Gupta and Varshney correlation [16], depend on the $Heat_{Flux}$, described by Pioro correlation [17], Equation (37).

$$h_{boil} = \frac{k_{Water}}{l_*} * 1.39 * \left[Heat_{Flux} * \rho_{Water} * Cp_{Water} * \frac{l_*}{\rho_l * h_{lv} * k_{Water}} \right]^{0.7} * \left(\rho_l / \rho_v \right)^{0.21} * \left(\mu_{Water} * \frac{Cp_{Water}}{k_{Water}} \right)^{-0.21} \tag{36}$$

$$Heat_{Flux} = \mu_{Water} * h_{lv} * l_* * \left[\left(\frac{1.0}{C_{sf}} \right)^{0.33} * \left(Pr_{Water} \right)^{1.0/0.33} * \left(Cp_{Water} * \frac{\Delta T_{Evsat}}{h_{lv}} \right)^{1.0/0.33} \right] \tag{37}$$

where,

$$l_* = \left[\frac{\sigma_{Water}}{g * \left(\rho_l - \rho_v \right)} \right]^{1.0/2.0} \tag{38}$$

The Nusselt number associated with air is represented by Equation (39).

$$Nu_{airEv} = 0.696 * \left(Re_{AirEv} \right)^{0.5} * \left(Pr_{air} \right)^{0.36} * \left(\frac{Pr_{air}}{5.0 * Pr_{air}} \right)^{0.25} \tag{39}$$

The heat transfer coefficient by air convection in the evaporator is obtained by:

$$h_{Ev} = Nu_{air} * \frac{k_{air}}{D_{ext}} \tag{40}$$

The application of the concept of "Aleta Analogy", conceived by Fakheri [1] leads us to define the following parameters:

$$mL_{EvFin} = \sqrt{\frac{2h_{Ev}}{k_{Fin} t_{Fin}}} P_{hEv} \tag{41}$$

$$\eta_{EvFin} = \frac{\mathrm{Tanh}\left(mL_{EvFin} \right)}{mL_{EvFin}} \tag{42}$$

The fin efficiency for the evaporator section is defined through Equation (42) by η_{EvFin}.

$$\beta_{Ev} = \frac{A_{trFin}}{A_{totEv}} \tag{43}$$

$$\eta'_{EvFin} = \beta_{Ev}\eta_{EvFin} + (1-\beta_{Ev}) \tag{44}$$

The efficiency associated with the set of fins in the evaporator, weighted by the area of change of the fins η'_{EvFin}, is represented through Equation (44).

$$Uo_{Ev} = \frac{1}{\frac{1}{h_{boil}} + \frac{D_{ext} - D_{int}}{k_W} + \frac{1}{\eta'_{EvFin} h_{Evair}}} \tag{45}$$

The global heat transfer coefficient associated with air in the evaporator, Uo_{Ev}, is given by Equation (45).

$$C_{Air} = \dot{m}_{air} Cp_{air} \tag{46}$$

The heat capacity of the air in the evaporator, C_{Air}, is given by Equation (46).

$$C_{Ev} = C_{air} \tag{47}$$

$$NTU_{Ev} = \frac{Uo_{Ev} * A_{totEv}}{C_{Ev}} \tag{48}$$

The number of thermal units associated with air in the evaporator, NTU_{Ev}, is given by Equation (48).

$$Fa_{Ev} = \frac{NTU_{Ev}}{2.0} \text{ for parallel flow} \tag{49}$$

The dimensionless number, called "fin analogy," Fa_{Ev} is represented by Equation (49) as defined by Ahamad Fakheri [12] and reported by Nogueira, É. [9]-[11].

$$\eta_{TEv} = \frac{\tanh(Fa_{eV})}{Fa_{Ev}} \tag{50}$$

The thermal efficiency associated with the evaporator is η_{TEv} [9]-[11].

$$\varepsilon_{TEv} = \frac{1}{\frac{1}{\eta_{tEv} NTU_{Ev}} + \frac{1}{2}} \tag{51}$$

The thermal effectiveness associated with the heat evaporator is ε_{TEv}.

$$\dot{Q}_{Ev} = \frac{C_{Ev}\Delta T_{Evsat}}{\frac{1}{\eta_{TEv} NTU_{Ev}} + \frac{1}{2}} \tag{52}$$

The heat transfer rate between the air and the heat pipe in the evaporating region $\dot{Q}_{Ev}$ is given by Equation (52).

$$T_{airout} = T_{airin} - \frac{\dot{Q}_{Ev}}{C_{Ev}} \tag{53}$$

After passing through the evaporator (precooling), the outlet air temperature is represented through Equation (53).

Thermal irreversibility in the evaporator is obtained using Equation (54), below.

$$Irrev_{TEv} = \log\left(\frac{T_{airin}}{T_{airout}}\right) \tag{54}$$

The rate of thermal entropy generation is represented by Equation (55).

$$\dot{S}gen_{TEv} = Irrev_{TEv} * C_{Ev} \tag{55}$$

$$Fric_{Ev} = \frac{0.31}{\left(Re_{AirHP}\right)^{0.25}} \tag{56}$$

The friction factor in the evaporator is represented by Equation (56).

$$\Delta p_{Ev} = Fric_{Ev} * \frac{L_{Ev}}{D_{hEv}} * \frac{\rho_{Air} * \left(V_{AirEv}\right)^{2.0}}{2} \tag{57}$$

The pressure drops across the evaporator is represented by Equation (57).

The pressure at the evaporator inlet is represented by Equation (58).

$$P_{1Ev} = P_{2Ev} + \Delta p_{Ev} \tag{58}$$

where,

$$P_{2Ev} = P_{atm} \tag{59}$$

Viscous irreversibility in the evaporator is obtained using Equation (60) below.

$$Irrev_{VEv} = \log\left(\frac{P_{2Ev}}{P_{1Ev}}\right) \tag{60}$$

The rate of viscous entropy generation is represented by Equation (61).

$$\dot{S}gen_{VEv} = Irrev_{VEv} * C_{Ev} \tag{61}$$

The Bejan number in the evaporator is represented by Equation (62).

$$Be_{Ev} = \frac{\dot{S}gen_{TEv}}{\dot{S}gen_{TEv} + \dot{S}gen_{VEv}} \tag{62}$$

3.2. Condenser

Table 3 shows the air properties as a function of the air inlet temperature at the condenser.

Table 3. Air properties as a function of condenser air inlet temperature.

T_{airin} °C	ρ_{air} Kg/m³	k_{air} W/(m·K)	Cp_{air} J/(kg·K)	Pr	μ_{air} Pa·s	ϑ_{air} m²/s	α_{air} m²/s
18.0	1.219	2.59×10^{-2}	1004.94	7.64×10^{-1}	1.97×10^{-5}	1.61×10^{-5}	2.11×10^{-5}
20.0	1.219	2.60×10^{-2}	1005.08	7.61×10^{-1}	1.9710^{-5}	1.61×10^{-5}	2.12×10^{-5}
22.0	1.219	2.61×10^{-2}	1005.22	7.58×10^{-1}	1.97×10^{-5}	1.62×10^{-5}	2.13×10^{-5}
24.0	1.219	2.63×10^{-2}	1005.36	7.55×10^{-1}	1.97×10^{-5}	1.62×10^{-5}	2.14×10^{-5}
26.0	1.219	2.64×10^{-2}	1005.49	7.52×10^{-1}	1.98×10^{-5}	1.62×10^{-5}	2.16×10^{-5}

The heat exchange area of the heat pipes in the condenser is represented by Equation (63).

$$A_{trCd} = L_{Cond} * N_{HP} * \left(P_{HP} - N_{Fin} * T_{Fin}\right) \tag{63}$$

The heat exchange area in the condenser is represented by Equation (64).

$$A_{totCd} = A_{trFin} + A_{trCd} \tag{64}$$

The Reynolds number associated with the air flow inside the condenser is represented by Equation (65).

$$Re_{AirCd} = \frac{4.0 * \dot{m}_{air}}{\pi * D_{hHP} * \mu_{air}} \tag{65}$$

The air velocity inside the condenser is represented by Equation (66).

$$V_{AirCd} = \frac{Re_{AirCd} * \mu_{air}}{D_{hHP}} \tag{66}$$

The saturation temperature difference across the condenser is represented by Equation (67).

$$\Delta T_{Cdsat} = T_{sat} - T_{airin} \tag{67}$$

The condensation coefficient in the condenser is represented by Equation (68).

$$h_{Cond} = 0.943 * \left(\frac{\rho_l * (\rho_l - \rho_v) * h_{lv} * g * (k_{water})^3}{\mu_{awter} * L_{Cd} * \Delta T_{Cdsat}} \right)^{1/4} \tag{68}$$

The Nusselt number associated with the air in the condenser is represented by Equation (69).

$$Nu_{airCd} = 0.696 * (Re_{AirCd})^{0.5} * (Pr_{air})^{0.36} * \left(\frac{Pr_{air}}{5.0 * Pr_{air}} \right)^{0.25} \tag{69}$$

The heat convection coefficient associated with the air in the condenser is represented by Equation (70).

$$h_{Cd} = Nu_{airCd} * \frac{k_{air}}{D_{ext}} \tag{70}$$

The application of the concept of "Aleta Analogy", conceived by Fakheri [1] leads us to define the following parameters:

$$mL_{CdFin} = \sqrt{\frac{2h_{Ev}}{k_{Fin} t_{Fin}}} P_{hCd} \tag{71}$$

$$\eta_{CdFin} = \frac{\mathrm{Tanh}(mL_{CdFin})}{mL_{CdFin}} \tag{72}$$

The fin efficiency for the condenser section is defined through Equation (72) by η_{CdFin}.

$$\beta_{Cd} = \frac{A_{trFin}}{A_{totCd}} \tag{73}$$

$$\eta'_{CdFin} = \beta_{Cd} \eta_{CdFin} + (1 - \beta_{Cd}) \tag{74}$$

The efficiency associated with the set of fins in the condenser, weighted by the area of change of the fins η'_{EvFin}, is represented through Equation (74).

$$Uo_{Cd} = \frac{1}{\frac{1}{h_{cond}} + \frac{D_{ext} - D_{int}}{k_W} + \frac{1}{\eta'_{CdFin} h_{Cd}}} \tag{75}$$

The global heat transfer coefficient associated with air in the condenser, Uo_{Cd}, is given by Equation (75).

$$C_{Air} = \dot{m}_{air} Cp_{air} \tag{76}$$

The heat capacity of the air in the condenser, C_{Air}, is given by Equation (76).

$$C_{Cd} = C_{air} \tag{77}$$

$$NTU_{Cd} = \frac{Uo_{Cd} * A_{totCd}}{C_{Cd}} \tag{78}$$

The number of thermal units associated with air in the condenser, NTU_{Cd}, is given by Equation (78).

$$Fa_{Cd} = \frac{NTU_{Cd}}{2.0} \text{ for counter flow} \tag{79}$$

The dimensionless number, called "fin analogy," Fa_{Cd} is represented by Equation (79) as defined by Ahamad Fakheri [1] and reported by Nogueira, É. [11]-[13].

$$\eta_{TCd} = \frac{\tanh\left(Fa_{Cd}\right)}{Fa_{Cd}} \tag{80}$$

The thermal efficiency associated with the condenser is η_{TCd}.

$$\varepsilon_{TCd} = \frac{1}{\frac{1}{\eta_{tCd} NTU_{Cd}} + \frac{1}{2}} \tag{81}$$

The thermal effectiveness associated with the condenser is ε_{TCd}.

$$\dot{Q}_{Cd} = \frac{C_{Cd} \Delta T_{Evsat}}{\frac{1}{\eta_{TCd} NTU_{Cd}} + \frac{1}{2}} \tag{82}$$

The heat transfer rate between the air and the heat pipe in the condenser region $\dot{Q}_{Cd}$ is given by Equation (82).

$$T_{airout} = \frac{\dot{Q}_{Cd}}{C_{Cd}} + T_{airin} \tag{83}$$

After passing through the condenser (heat recover), the outlet air temperature is represented through Equation (83).

Thermal irreversibility in the condenser is obtained using Equation (84) below.

$$Irrev_{TCd} = \log\left(\frac{T_{airin}}{T_{airout}}\right) \tag{84}$$

The rate of thermal entropy generation in the condenser is represented by Equation (85).

$$\dot{S}gen_{TCd} = Irrev_{TCd} * C_{Cd} \tag{85}$$

$$Fric_{Cd} = \frac{0.31}{\left(Re_{AirCd}\right)^{0.25}} \tag{86}$$

The friction factor in the condenser is represented by Equation (86).

$$\Delta p_{Cd} = Fric_{Cd} * \frac{L_{Cd}}{D_{hCd}} * \frac{\rho_{Air} * \left(V_{AirCd}\right)^{2.0}}{2} \tag{87}$$

The pressure drops across the condenser is represented by Equation (87).

The pressure at the evaporator inlet is represented by Equation (88).

$$P_{1Cd} = P_{2Cd} + \Delta p_{Cd} \tag{88}$$

By definition:

$$P_{2Cd} = P_{atm} \tag{89}$$

Viscous irreversibility in the condenser is obtained using Equation (90) below.

$$Irrev_{VCd} = \log\left(\frac{P_{2Cd}}{P_{1Cd}}\right) \tag{90}$$

The rate of viscous entropy generation in the condenser is represented by Equation (91).

$$\dot{S}gen_{VCd} = Irrev_{VCd} * C_{Cd} \tag{91}$$

The Bejan number in the condenser is represented by Equation (92).

$$Be_{Cd} = \frac{\dot{S}gen_{TCd}}{\dot{S}gen_{TCd} + \dot{S}gen_{Cd}} \tag{92}$$

4. Results and Discussion

4.1. Evaporator

This section presents results for thermal and viscous performances related to the evaporator of the axially finned heat pipe heat exchanger, for configurations with 29 and 47 heat pipes.

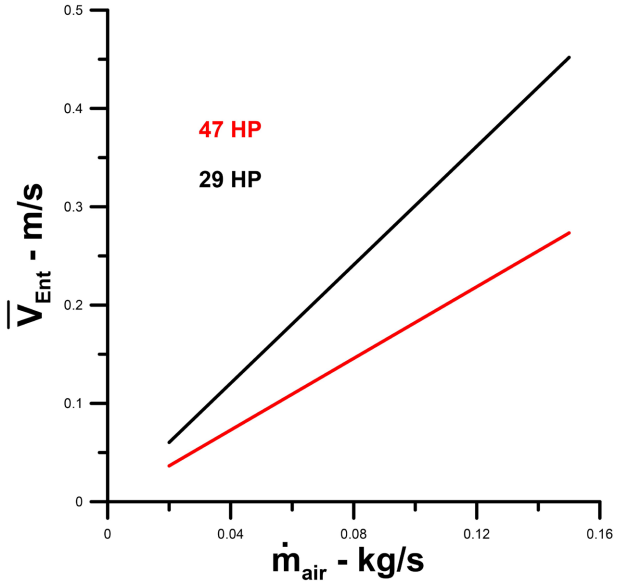

Figure 3. Velocidade do ar na entrada do evaporador versus vazão em massa.

Figure 3 presents the average air velocities for the two configurations considered in this work, with shell diameters equal to 614 mm (29 heat pipes) and 789 mm (47 heat pipes). As expected, the inlet velocity of the heat exchanger with the larger diameter has a lower velocity.

Figure 4 shows the average velocity inside the heat exchangers considered in the evaporator analysis. As expected, due to its larger equivalent diameter, the heat exchanger with 47 heat pipes has a lower internal velocity, despite the larger area occupied by the heat pipes and fins. Figure 2 shows a cross-sectional representation of the finned heat pipes arranged symmetrically inside the shell for the 29-heat pipe configuration. The radial configuration is designed to achieve homogeneous air distribution inside the heat exchanger.

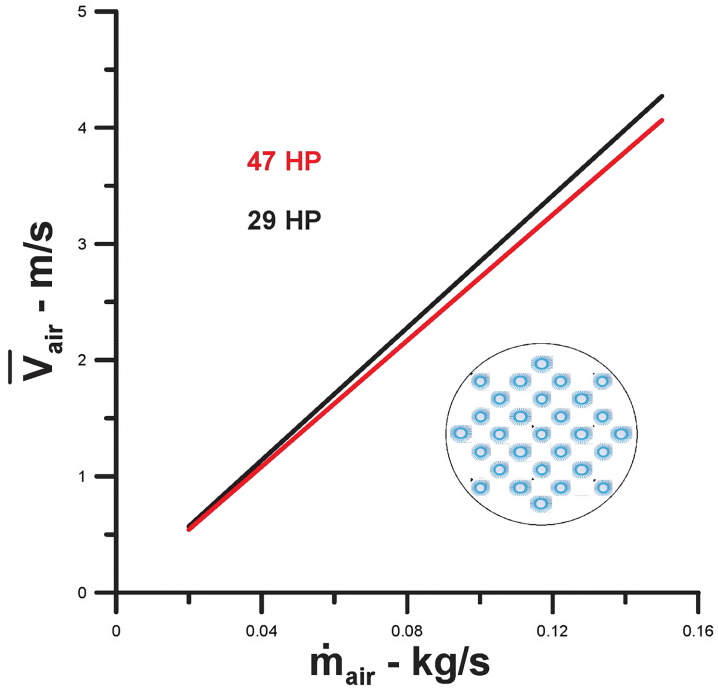

Figure 4. Average air velocity inside the evaporator versus air mass flow rate.

The maximum permissible velocity inside the heat exchanger is 6 m/s. This value limits the flow rate that can be used. For a 49-tube heat exchanger, this value is achieved with a mass flow rate of 0.2 kg/s. A standard 60 m^3 operating room with 20 air changes per hour, as defined by country-specific standards, requires a flow rate of 0.4 kg/s. In this case, two 49-tube heat exchangers are needed to meet the pre-established requirements.

As expected, the Reynolds number in the evaporator, represented in Figure 5, demonstrates a similar trend to the internal velocity in the evaporator, with the heat exchanger with 47 heat pipes presenting slightly lower values for higher air flows.

The Nusselt number, Figure 6, presents results like those obtained and represented in Figure 3, as it is strongly dependent on the Reynolds number.

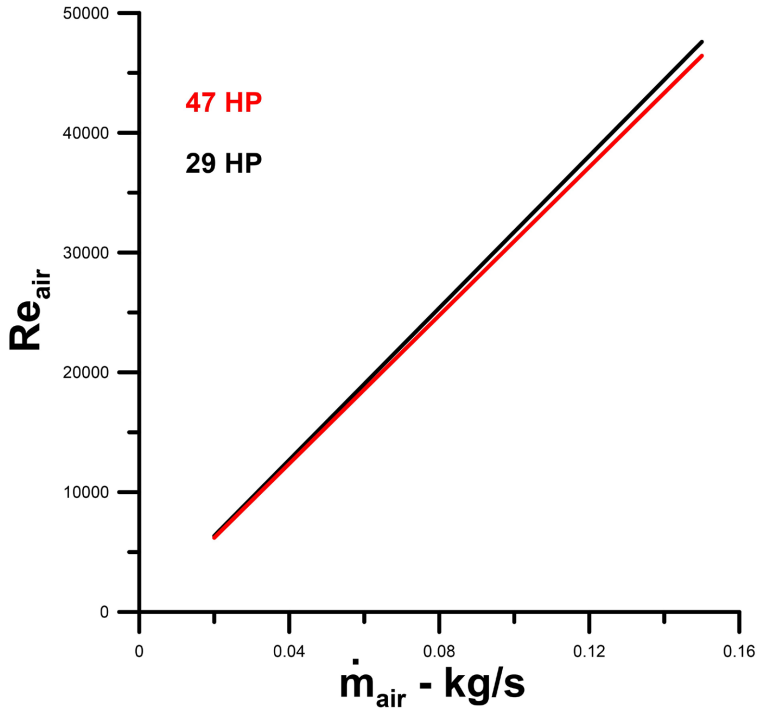

Figure 5. Evaporator Reynolds number versus air mass flow rate.

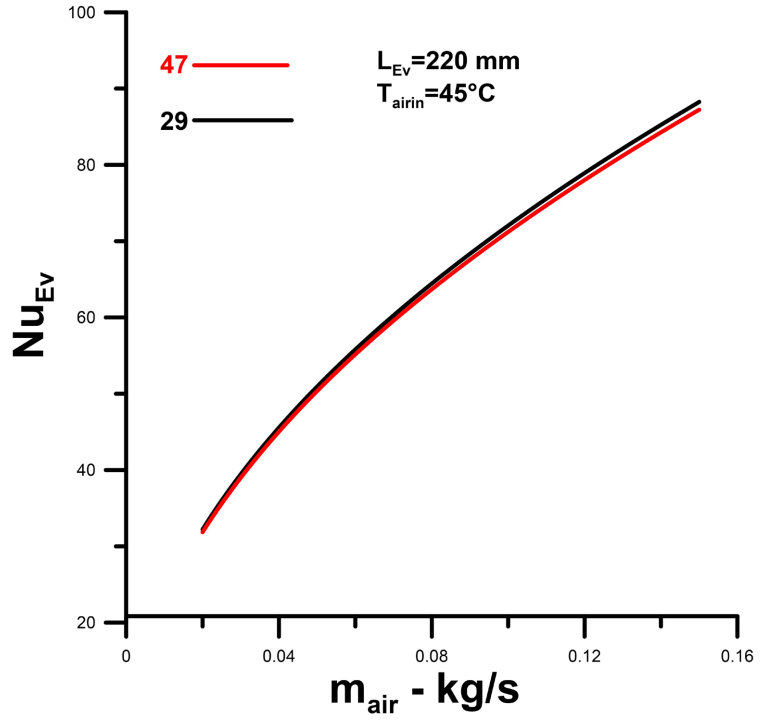

Figure 6. Evaporator Nusselt number versus air mass flow rate.

Figure 7 presents values for the boiling heat transfer coefficient. The boiling coefficient presents significantly higher values with increasing air temperature, since it depends on the temperature difference between the air inlet temperature

and the saturation temperature of the working fluid.

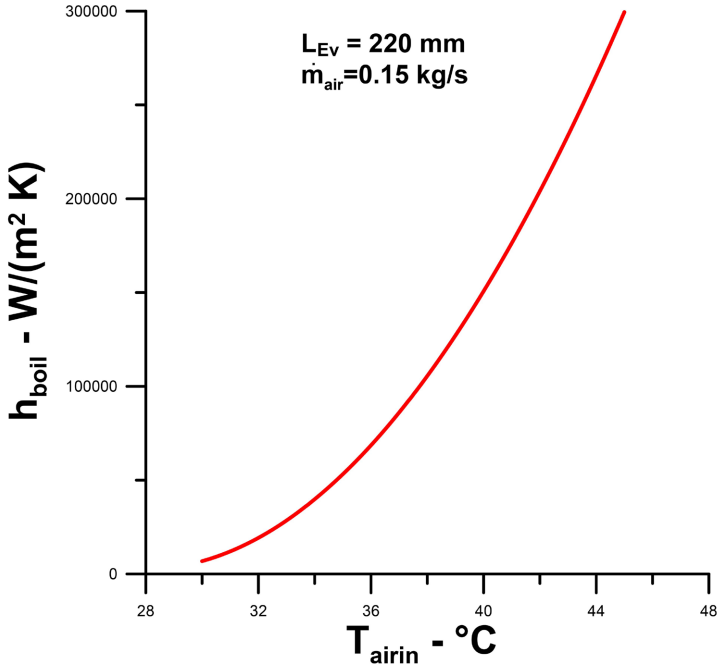

Figure 7. Boiling heat transfer coefficient versus air inlet temperature.

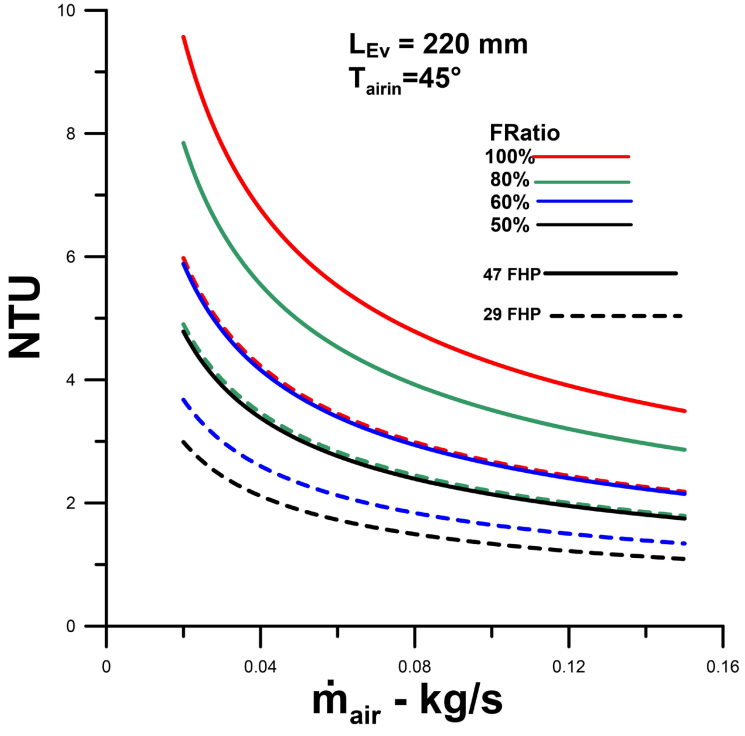

Figure 8. Number of thermal units versus air mass flow rate.

The number of thermal units in the evaporator is represented in Figure 8, as a function of the air inlet flow rate and for the maximum temperature, equal to

45˚C. The working fluid filling ratio in the heat pipes, in purely theoretical terms, varies from 50% to 100%. The number of thermal units increases with the filling rate, and the number of heat pipes and decreases with an increasing flow rate. The increase in the number of heat pipes can be explained by the increase in the heat exchange area, and the increase in the filling rate is explained by the higher value of the overall heat exchange coefficient, which is strongly dependent on the boiling coefficient.

Figure 9 presents result for evaporator thermal effectiveness, for an air inlet temperature of 45˚C and a working fluid fill ratio ranging from 50% to 100%. As expected, thermal effectiveness presents results like those of the number of thermal units, since it is strongly dependent on this parameter. What stands out in the results obtained are the high thermal effectiveness values across the entire flow rate range under analysis. The extremely high effectiveness values, even for a working fluid fill ratio of 50%, demonstrate that the 47-finned heat pipe configuration has great potential for use in air conditioning systems for thermal comfort. Even for the 29-tube configuration, the results presented, for a fill ratio of 60%, are extremely promising.

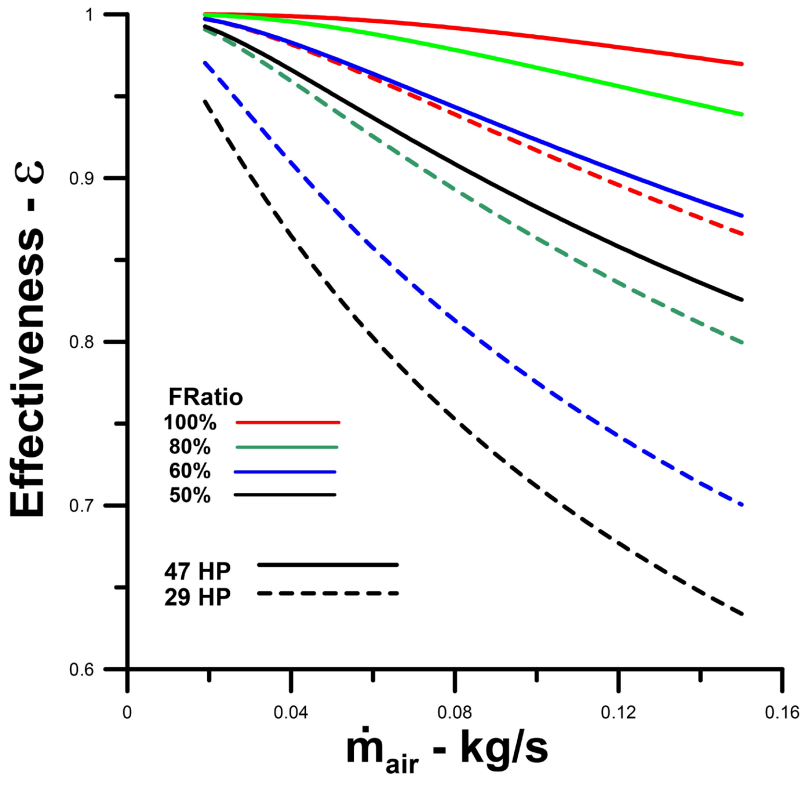

Figure 9. Thermal effectiveness versus air mass flow rate and with filling fraction as a parameter.

The heat transfer rate in the evaporator, for an air inlet temperature of 45˚C, is represented in Figure 10. The results obtained reflect what was observed for thermal effectiveness, with higher values for a greater number of heat pipes and higher

working fluid filling rates. It should be noted that the analysis is restricted to the final position of the evaporator contained by the working fluid, since this is the most relevant region in terms of heat exchange.

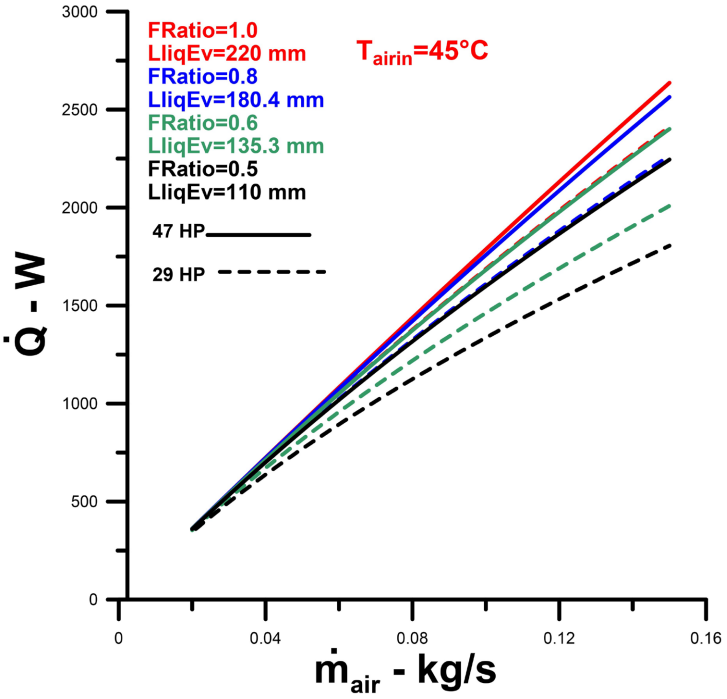

Figure 10. Heat transfer rate versus air mass flow rate and with filling ratio as a parameter.

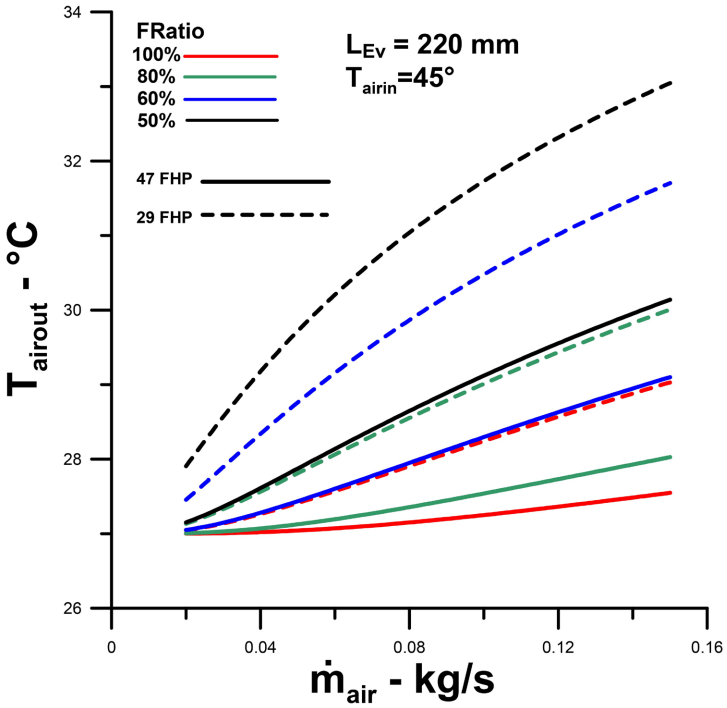

Figure 11. Air outlet temperature versus air mass flow rate and with filling ratio as a parameter.

The air outlet temperature is represented in Figure 11. The results obtained for the 47-finned heat pipe configuration, as expected, are extremely promising, since the temperature, for a 60% fill ratio, presents outlet temperatures between 27˚C and 28˚C, for almost the entire flow rate range under analysis. Even for the 29-tube configuration, the results obtained for a fill fraction of 80%, below 30˚C and an air inlet temperature of 45˚C, demonstrate exceptional thermal performance for the theoretical design of the heat exchanger under analysis.

The current design, with axially finned heat pipes, is compared with the design of radially finned heat pipes, whose theoretical-experimental study is described through the work presented by Ragil Sukarno *et al.* [3], and a comparative theoretical study, through the Thermal Efficiency Method, carried out by Élcio Nogueira [11].

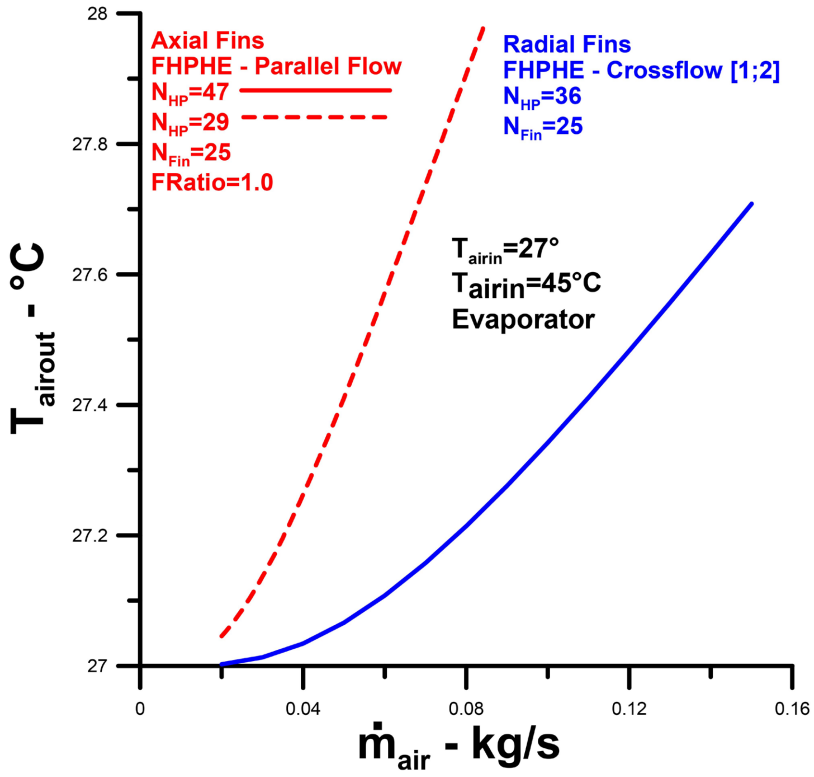

Figure 12. Air outlet temperature versus air mass flow rate for radial and axial finned heat exchanger configurations.

The results of the comparison performed in this work are shown in Figure 12, for air outlet temperature as a function of flow rate. It can be observed that the axial design with 47 finned heat pipes presents better thermal performance than the radial configuration, for a fill ratio of 100%. However, for an effective comparison, the heat exchange areas of each heat exchanger design must be analyzed: For 29 axially finned heat pipes, with 25 fins per tube, the total heat exchange area in the evaporator is 0.17 m^2; for 47 axially finned heat pipes, with 25 fins per tube, the total heat exchange area in the evaporator is 0.27 m^2; in the case of radially

finned heat pipes, the total heat exchange area in the evaporator is 0.39 m^2. In terms of thermal performance in the evaporator, the axially finned tube design offers better performance, as it provides superior results for a smaller heat exchange area.

The results and analyses presented for thermal performance, in the evaporator, validate and demonstrate better thermal performance for the current configuration.

A heat exchanger analysis, which takes into account the cost-benefit in terms of thermal/viscous performance, is presented below for the evaporator.

Figure 13 presents the coefficient of friction results for the two designs analyzed in this work: axially finned heat pipes with 29 tubes and 47 tubes, both with 25 fins per tube. Since the design with the greater number of tubes and fins has a larger area, it would be expected to have a significantly higher coefficient of friction. However, it can be seen that the velocity (Figure 4) is lower for the greater number of tubes, since the air passage area is larger. This characteristic balances the coefficient of friction results, making the result obtained for 47 tubes slightly higher than the result obtained for 29 heat pipes. As will be discussed later, this result has a positive impact on thermal/viscous performance in the current configuration.

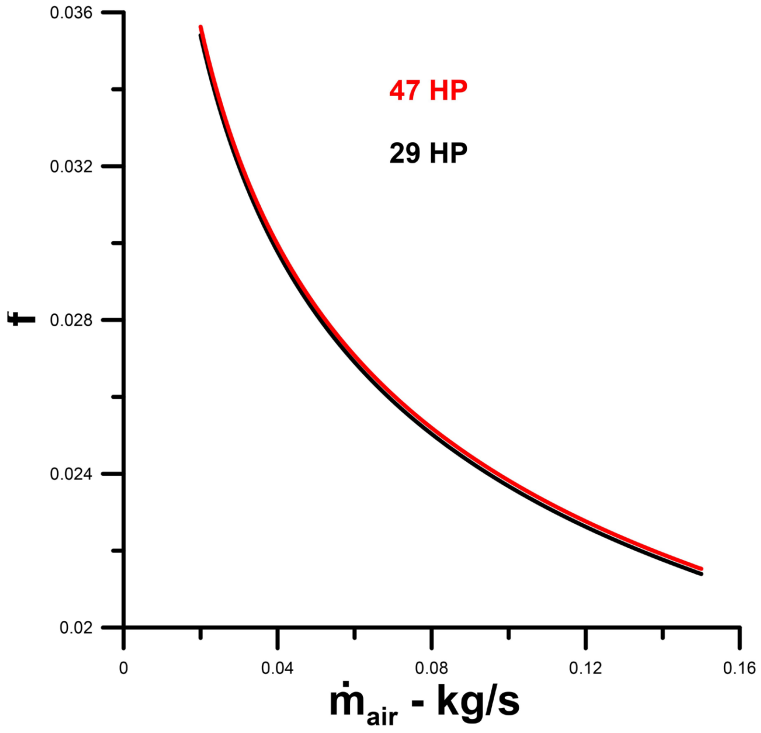

Figure 13. Friction factor versus air mass flow rate.

The results for evaporator pressure drop are shown in Figure 14. The pressure drop for the 47-tube configuration shows a lower pressure drop than that for the 29-tube configuration. These results reflect what was observed for internal veloc-

ities in the heat exchanger, since the larger the number of tubes, the larger the air passage area.

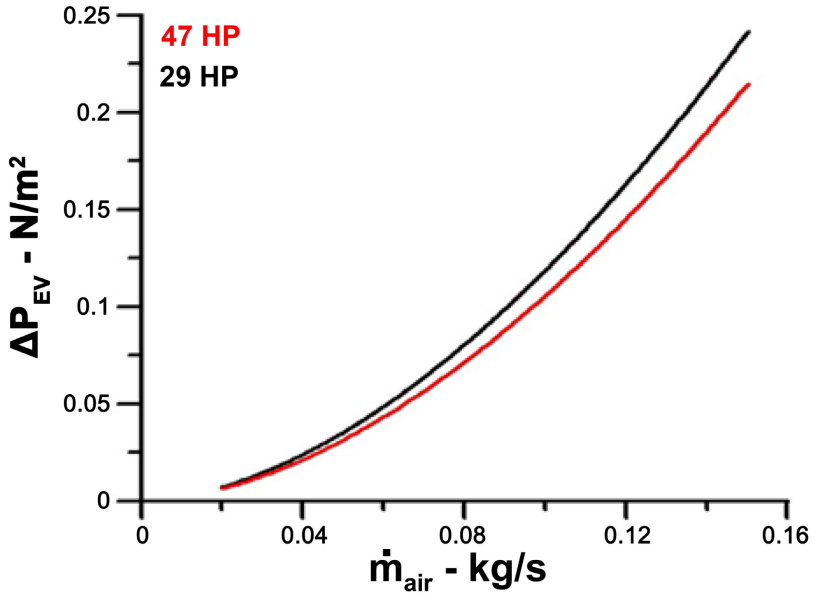

Figure 14. Pressure drops versus mass flow rate.

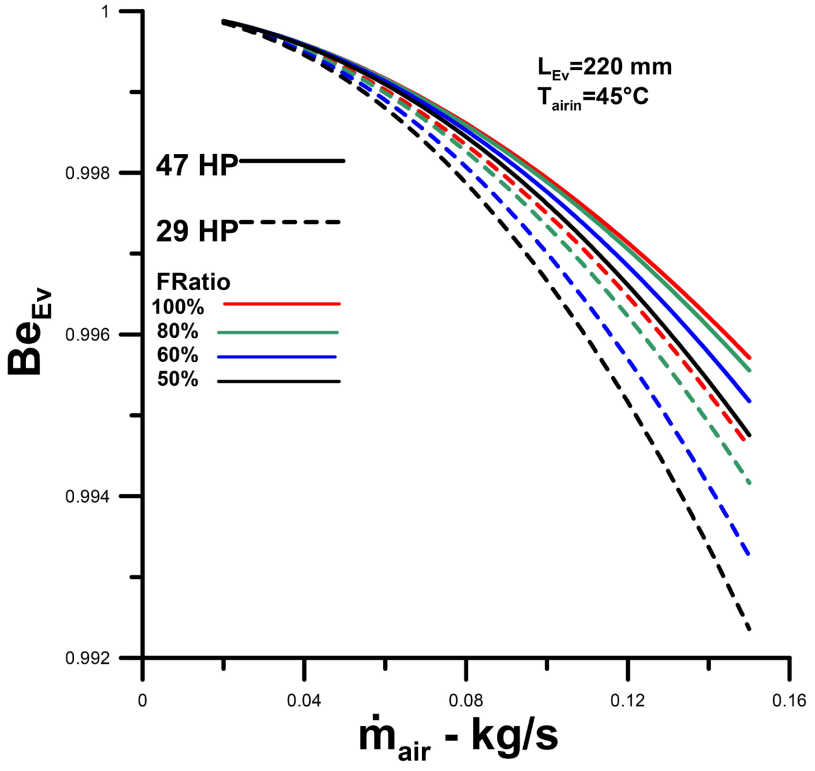

Figure 15. Bejan number versus mass flow rate with working fluid filling ratio as parameter.

The results for the evaporator's Bejan number are presented in **Figure 15** for

the two configurations under analysis: 29 and 47 axially finned heat pipes. Initially, the significant superiority of the 47-heat pipe design can be observed, as it offers a higher Bejan number for a given air mass flow rate. In this case, the result reflects higher thermal performance and lower pressure loss for the 47-heat pipe configuration. However, what is very favorable, in terms of cost-benefit, is that the value obtained is extremely high for both cases. These results demonstrate that the heat exchanger designs analyzed are extremely promising, as they offer high heat transfer rates and low pressure drops.

4.2. Condenser

This section presents results for thermal and viscous performances related to the condenser of the axially finned heat pipe heat exchanger, for configurations with 29 and 47 heat pipes.

The results obtained for the condenser are very similar to those obtained for the evaporator. Numerically, however, they present different values, since the length of the condenser is equal to half the length of the evaporator, and the temperature differences between the air inlet temperature and the saturation temperature are smaller. The air inlet temperature to the evaporator varies between 18˚C and 26˚C.

The air velocity values inside the condenser (Figure 16) are lower than those observed for the evaporator, due to the condenser's smaller hydraulic diameter. The velocity values for the 47-heat pipe configuration, which has a larger air passage area, are reflected in lower velocity values.

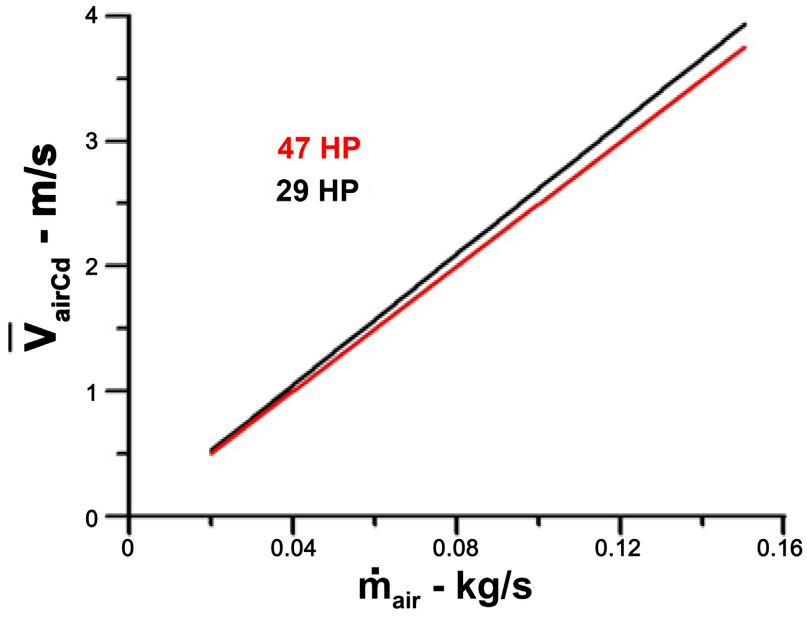

Figure 16. Average air velocity in the condenser versus air mass flow rate.

Figure 17 presents result for the condensation heat transfer coefficient. The values are lower than those obtained for the boiling coefficient, due to the high

heat transfer resistance presented by the water vapor fraction inside the heat pipes. This result is expected to impact the condenser's thermal performance.

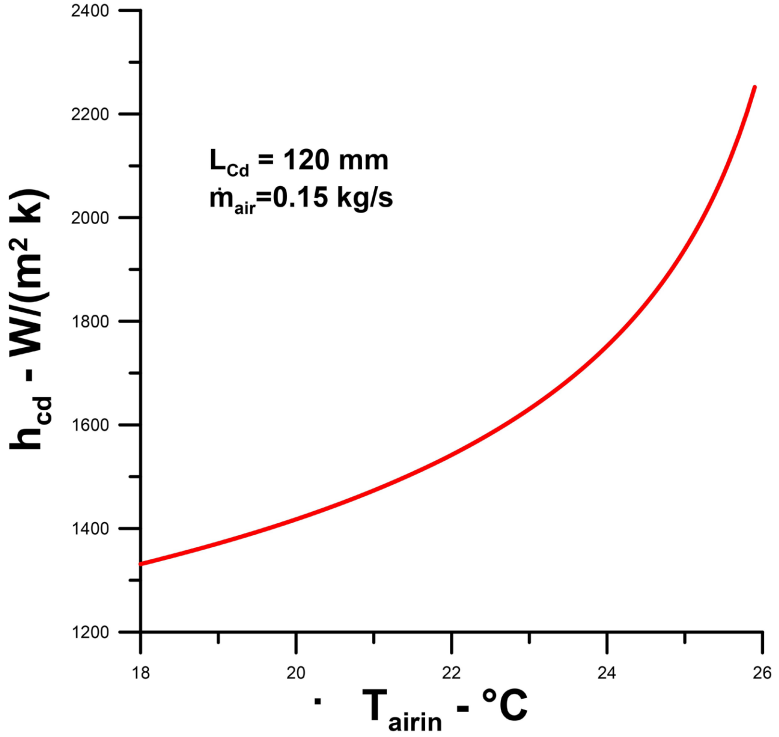

Figure 17. Heat transfer coefficient by condensation versus air input temperature.

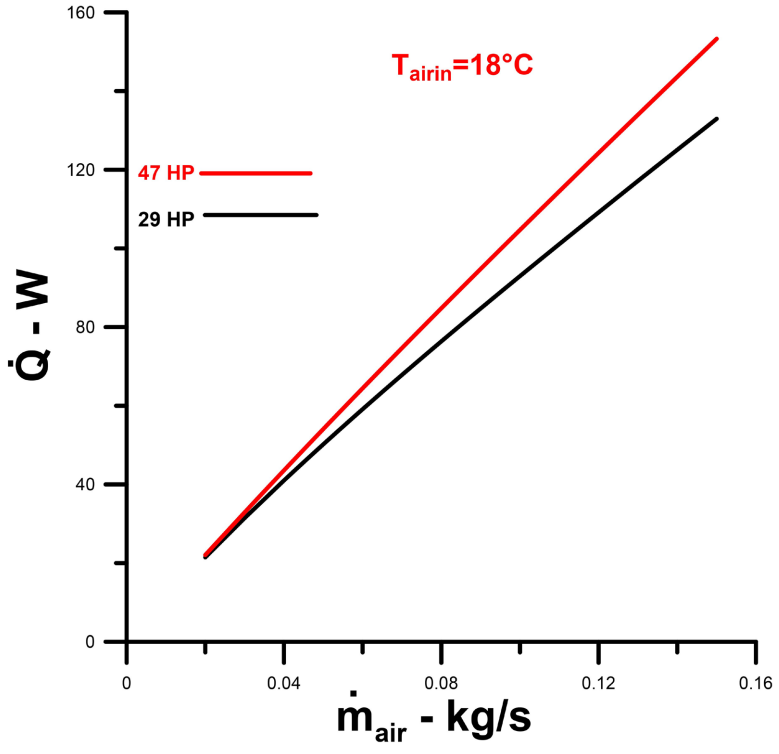

Figure 18. Condenser heat transfer rate versus air mass flow rate.

Figure 18 presents the results for the condenser heat transfer rate as a function of the air mass flow rate for the two configurations under analysis. The input parameter is an air temperature of 18˚C. The condenser heat transfer rate is higher for the 47-heat pipe design due to the larger heat exchange area.

A comparison between axially finned and radially finned heat pipe designs for evaporator outlet air temperature is shown in Figure 19. The thermal performance of the axially finned heat pipe configurations is significantly superior for both 29-tube and 47-tube configurations. The results obtained for the condenser are qualitatively different from those obtained for the evaporator. The numerical superiority of the 47-tube heat pipe configuration is explained by the larger heat exchange area, in relation of the 29-tube heat exchanger. The superiority of the 29-tube configuration, compared to the crossflow arrangement, despite the greater number of heat pipes, can be explained by the heat exchanger configuration. In the condenser, the countercurrent flow configuration offers superior thermal performance compared to the parallel flow configuration, as in the evaporator. Another relevant aspect is that the hydraulic diameter in the condenser is smaller than that of the evaporator, and this affects the external flow in relation to the heat pipes, increasing the Reynolds number.

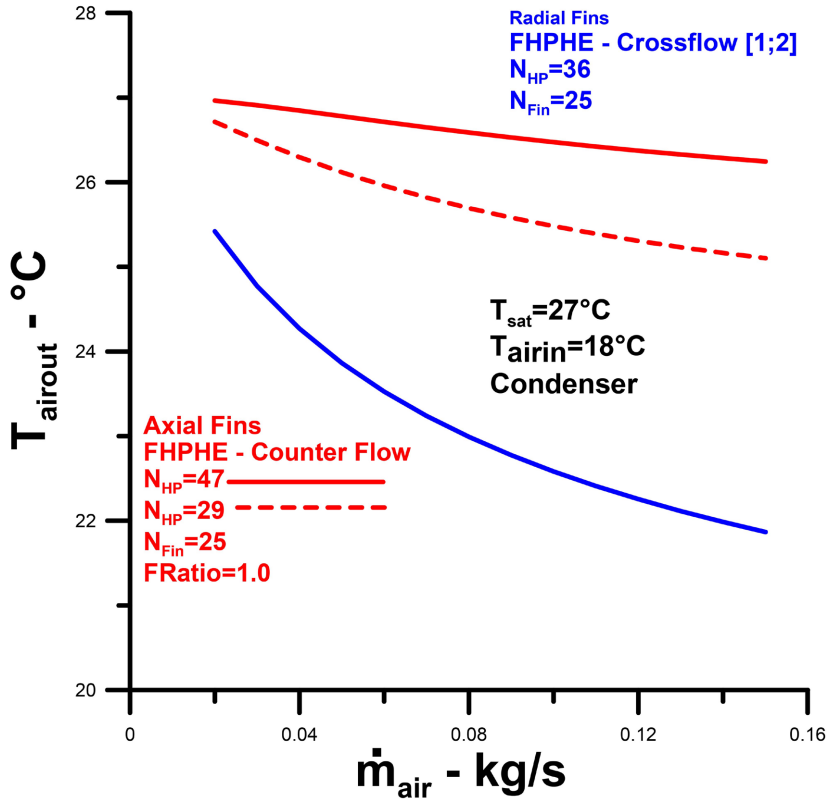

Figure 19. Comparison of condenser outlet air temperature versus air mass flow rate for radial and axial fin configurations.

The results presented for the Bejan number in the condenser are represented in

Figure 20. As expected, based on what was already discussed for the evaporator, the Bejan number is higher for the 47-tube configuration because it has a larger heat exchange area and air passage area. However, what is noteworthy, once again, is the thermal performance versus viscous dissipation, which is extremely high for both configurations analyzed. In this sense, the cost-benefit associated with the heat exchanger is very favorable, due to its high thermal performance.

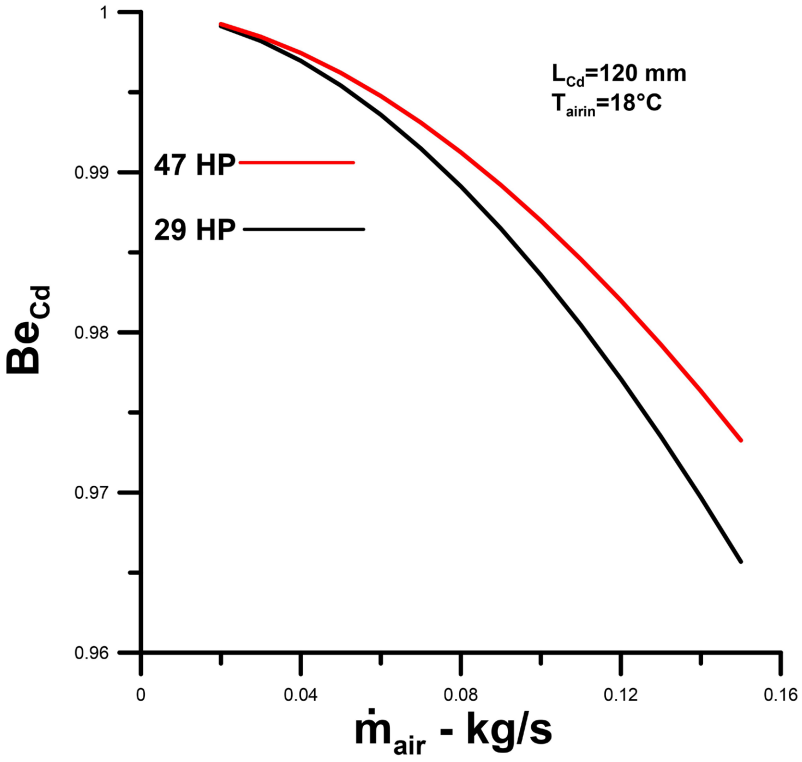

Figure 20. Bejan number in the condenser versus air mass flow rate.

4.3. Considerations on the Current AFTHE Configuration

The air outlet configurations in the heat exchanger under analysis, represented in Figures 2(a)-(c), are highlighted in the last one, as it more functionally encompasses the first two. Despite this, it cannot yet be considered definitive for two reasons: four air outlets, despite resulting in a completely symmetrical and functional configuration, are not a practical option when directing cooled or heated air to a given installation; and to achieve the final solution, due to the air-directing curves, it was necessary to extend the length of the adiabatic region (200 mm). This length does not correspond to the length of the adiabatic region (120 mm) considered in the simulation, since it was decided to maintain the dimensions of the heat exchanger that had already demonstrated satisfactory experimental results and was the subject of comparison in this work.

If the heat exchanger outlet area is included in the heat exchanger analysis, its viscous dissipation must be added to the viscous dissipation rate determined for the evaporator and condenser lengths, which will negatively affect the overall per-

formance of the heat exchanger. In this case, the Bejan number should decrease, since the total irreversibility, thermal + viscous, increases. To minimize this undesirable but unavoidable effect, the air outlet should be designed to minimize viscous losses as much as possible. However, expectations in this case are positive since the heat exchange performance is exceptionally high.

5. Conclusions

This paper presents graphical results for an axially finned heat pipe heat exchanger in two configurations: 29 and 47 heat pipes, in the evaporator and condenser. Furthermore, a comparison is presented between two distinct heat exchangers with very similar physical characteristics in terms of air mass flow rate, air inlet temperatures, working fluid and saturation temperature. The significant differences between the two types of heat exchangers relate to the physical arrangement of the fins on the heat pipes and the number of heat pipes. The work used for comparison consists of radially finned heat pipes. Furthermore, the results used for comparison were validated by different numerical models and experimental results.

The analysis method used in this work consists of an analytical model called the Thermal Efficiency Method, already consolidated, based on numerous theoretical-experimental comparisons carried out over the last few years.

The analysis concludes that the thermal and viscous performance of the heat exchangers designed is very promising. These results are reflected in the high Bejan number obtained for the two configurations under analysis: 29 and 47 axially finned heat pipes. The Bejan number ultimately represents the relationship between thermal performance and the overall performance of the heat exchanger.

Thermal performance is high compared to viscous dissipation, resulting in a very favorable cost-benefit ratio for the heat exchanger under analysis.

The results demonstrate significant potential for the construction and testing of a heat exchanger with axial fins to obtain experimental results and for theoretical and experimental comparisons of parameters related to the heat exchangers under analysis.

It is important to note, however, that pressure drops across the air outlets were not considered in the simulation, and the results presented for viscous dissipation were applicable only to the evaporator and condenser dimensions. Air outlets, when finally installed, are expected to have a low economic impact on the heat exchanger.

Finally, it must be stated that the chosen application was not by chance, since the results presented satisfy the specific requirements of high thermal efficiency and low-pressure drop for the heat exchanger. These requirements are directly associated with the need for precise temperature control and efficient air circulation in the operating room air conditioning systems mentioned in the introduction.

In summary, the current theoretical project presents promising results and should be used in the experimental implementation of an air conditioning system

for surgical rooms.

Conflicts of Interest

The authors declare no conflicts of interest regarding the publication of this paper.

References

[1] Fakheri, A. (2007) Heat Exchanger Efficiency. *Journal of Heat Transfer*, **129**, 1268-1276. https://doi.org/10.1115/1.2739620

[2] Zimparov, V.D., Angelov, M.S. and Hristov, J.Y. (2021) Critical Review of the Definitions of the Bejan Number—First Law of Thermodynamics. *International Communications in Heat and Mass Transfer*, **124**, Article 105113. https://doi.org/10.1016/j.icheatmasstransfer.2021.105113

[3] Sukarno, R., Putra, N., Hakim, I.I., Rachman, F.F. and Mahlia, T.M.I. (2021) Multistage Heat-Pipe Heat Exchanger for Improving Energy Efficiency of the HVAC System in a Hospital Operating Room 1. *International Journal of Low-Carbon Technologies*, **16**, 259-267. https://doi.org/10.1093/ijlct/ctaa048

[4] Jouhara, H., Almahmoud, S., Brough, D., Guichet, V., Delpech, B., Chauhan, A., *et al.* (2021) Experimental and Theoretical Investigation of the Performance of an Air to Water Multi-Pass Heat Pipe-Based Heat Exchanger. *Energy*, **219**, Article 119624. https://doi.org/10.1016/j.energy.2020.119624

[5] Górecki, G., Łęcki, M., Gutkowski, A.N., Andrzejewski, D., Warwas, B., Kowalczyk, M., *et al.* (2021) Experimental and Numerical Study of Heat Pipe Heat Exchanger with Individually Finned Heat Pipes. *Energies*, **14**, Article 5317. https://doi.org/10.3390/en14175317

[6] Barrak, A. (2021) Heat Pipes Heat Exchanger for HVAC Applications. In: *Heat Transfer—Design, Experimentation and Applications*, IntechOpen, 1-14. https://doi.org/10.5772/intechopen.95530

[7] Putra, N.S.D., Anggoro, T. and Winarta, A. (2017) Experimental Study of Heat Pipe Heat Exchanger in Hospital HVAC System for Energy Conservation. *International Journal on Advanced Science, Engineering and Information Technology*, **7**, Article 871. https://doi.org/10.18517/ijaseit.7.3.2135

[8] Ibnu Hakim, I., Sukarno, R. and Putra, N. (2021) Utilization of U-Shaped Finned Heat Pipe Heat Exchanger in Energy-Efficient HVAC Systems. *Thermal Science and Engineering Progress*, **25**, Article 100984. https://doi.org/10.1016/j.tsep.2021.100984

[9] Yin, X., Wu, X.T., Zhou, S.F., Zhu, X.X. and Wang, N.H. (2023) Numerical Simulation of the Evaporator in Two–Phase Thermosyphon Loop for Passive Containment Cooling System. *Annals of Nuclear Energy*, **180**, Article 109506. https://doi.org/10.1016/j.anucene.2022.109506

[10] Eshwar, H., Arunachala, U.C. and Varun, K. (2024) Single-Phase Thermosyphon Heat Transport Device, a Future Prospect for Heat Removal Applications: An Experimental Comparison with Heat Pipe and Two-Phase Closed Thermosyphon. *International Journal of Thermal Sciences*, **203**, Article 109130. https://doi.org/10.1016/j.ijthermalsci.2024.109130

[11] Nogueira, É. (2023) Theoretical Thermal Performance of Cross-Flow Finned Heat Pipe Heat Exchanger Used for Air Conditioning in Surgery Rooms. *Mechanical Engineering Advances*, **1**, Article 131. https://doi.org/10.59400/mea.v1i1.131

[12] Nogueira, E. (2020) Thermal Performance in Heat Exchangers by the Irreversibility, Effectiveness, and Efficiency Concepts Using Nanofluids. *Journal of Engineering Sci-*

ences, **7**, F1-F7. https://doi.org/10.21272/jes.2020.7(2).f1

[13] Nogueira, E. (2025) Heat Exchangers: Analytical Modeling and Applications. Editora Dialética.

[14] Rohsenow, W.M. (1951) A Method of Correlating Heat Transfer Data for Surface Boiling of Liquids. Massachusetts Institute of Technology.

[15] Jouhara, H., Chauhan, A., Nannou, T., Almahmoud, S., Delpech, B. and Wrobel, L.C. (2017) Heat Pipe Based Systems—Advances and Applications. *Energy*, **128**, 729-754. https://doi.org/10.1016/j.energy.2017.04.028

[16] Hameed, M.S., Khan, A.R. and Mahdi, A.A. (2013) Modeling a General Equation for Pool Boiling Heat Transfer. *Advances in Chemical Engineering and Science*, **3**, 294-303. https://doi.org/10.4236/aces.2013.34037

[17] Pioro, I.L., Rohsenow, W. and Doerffer, S.S. (2004) Nucleate Pool-Boiling Heat Transfer. II: Assessment of Prediction Methods. *International Journal of Heat and Mass Transfer*, **47**, 5045-5057. https://doi.org/10.1016/j.ijheatmasstransfer.2004.06.020

Nomenclature

$Asec$ —cross-section area, [m^2]
Atr —heat transfer area, [m^2]
Cp —specific heat, [J/kg·K]
C —thermal capacity, [W/K]
$C_{\min}$ —minimum thermal capacity, [W/K]
$C^* = \frac{C_{\min}}{C_{\max}}$
D_h —hydraulic diameter, [m]
Fa —fin analogy
h —coefficient of heat convection, [W/m^2·K]
k —thermal conductivity, [W/m·K]
K —Kelvin
k_W —thermal conductivity of the tube, [W/m·K]
k_{Fin} —thermal conductivity of the fin, [W/m·K]
L —vertical or horizontal length, [m]
$\dot{m}_{air}$ —mass flow rate of the air, [kg/s]
N_{Fin} —number of fins
Nu —Nusselt number
Pr —Prandtl number
$\dot{Q}$ —actual heat transfer rate, [W]
$\dot{Q}_{\max}$ —maximum heat transfer rate, [W]
Re —Reynolds number
T —temperatures, [˚C]
Uo —global heat transfer coefficient, [W/m^2·K]

Subscripts

boil—ebulição
Cd—Condenser
Cond—Condenser
effect—effective
Ev—Evaporator
ext—external
HP—heat pipe
H—horizontal
in—inlet
int—internal
out—outlet
sat—saturation

Greek symbols

α —thermal diffusivity, [m^2/s]
β —the relationship between areas
ρ —density of the fluid, [kg/m^3]
μ —dynamic viscosity of fluid, [kg/m·s]

ν —kinematic viscosity of the cold fluid, [m²/s]
ε_T —thermal effectiveness
η_T —thermal efficiency
ΔT —a difference of temperatures, [˚C]
Acronyms
FHPHE—Finned heat pipe heat exchanger
Ev—Evaporators
Cd—Condenser
NHP—Number of Heat Pipes
NFin—Number of Fins
Nrows—Number of rows
NTU—number of thermal units